6th International Conference on Advances in Experimental Structural Engineering
11th International Workshop on Advanced Smart Materials and Smart Structures Technology
August 1-2, 2015, University of Illinois, Urbana-Champaign, United States

Electro-mechanical sensing performance of three-dimensional graphene aerogel multifunctional composites under ultra-large deformations

Q. Zhang[1], H. Li[2], X. Xu[3], Y. Yu[4]

1 *PhD candidate, Center of Structural Monitoring and Control,School of Civil Engineeing, Harbin Institute of Technology, China. Purdue University, West Lafayette, United States.*
Email:zhangqq_hit@126.com & zhan2040@purdue.edu
2 *Professor, Center of Structural Monitoring and Control,School of Civil Engineeing, Harbin Institute of Technology, China.*
E-mail: lihui@hit.edu.cn
3 *Assistant Professor, Center of Structural Monitoring and Control,School of Civil Engineeing, Harbin Institute of Technology, China.*
E-mail: xuxiang@hit.edu.cn
4 *Undergraduate, School of Civil Engineeing, Harbin Institute of Technology, China.*
E-mail: yuyikang@outlook.com

ABSTRACT
Utilizing large-scaled graphene oxide (LGO) sheets, three dimensional (3D) graphene aerogels (GAs) nanostructures were fabricated as a macroscopic monolithic from individual graphene sheets by modified hydrothermal reduction and followed by freeze-drying process. Due to Because of the well-interconnected 3D networks, larger stacking interfaces and strong π-π interactions between graphene sheets, GAs presents well-shaped and self-supported hierarchical nano nanostructures with high porosity, ultralight density, ultra-high and high electrical conductivity. By ice-bath assisted infiltration and vacuum curing process, GAs was incorporated with polydimethylsiloxane (PDMS) to fabricate conductive composites and explore extensive applications in macroscopic scale. Based on originally well-connected 3D conductive networks of graphene sheets, GA/PDMS composites (GAPCs), freeing from the constraints of matrix on conductive properties, exhibit excellent electro-mechanical and stable piezo-resistance effect, significant improvement of electrical (~ 1 S/cm). The multifunctional GAPC offers promise in applications such as stretchable electrodes and ultra-large strain sensors.

KEYWORDS: *graphene aerogels, modified hydrothermal reduction, ultra-high compressibility, piezo-resistance effect, GA/PDMS composites (GAPCs)*

1. INTRODUCTION

Graphene has attracted intense attention in both scientific and engineering fields in recent years because of its unique properties [1-3] such as high thermal conductivity (~ 5000 W/(m•K)) [4], large charge carrier mobility at low temperature (~ 200000 $cm^2/(V•s)$) [5], huge specific area (~ 2630 m^2/g) [6], excellent optical transparency (~ 97.7%) [7], and extraordinary elastic properties (Young's modulus ~ 1.0 TPa, fracture strength ~ 125 GPa) [8]. To exploit these outstanding nanoscale properties for macroscopic applications, graphene nanosheets are required to be synthesized at a large scale and assembled into monoliths. Many approaches to synthesize graphene or its derivatives have been developed, including chemical oxidation, mechanical exfoliation, chemical vapor deposition (CVD), intercalation and liquid sonication [1, 9-12]. Particularly because of the easy and scalable preparation process, low cost and promising chemical and mechanical properties, graphene oxide (GO) sheets are expected to be the suitable candidates to fabricate electrically and thermally conductive graphene-based macroscopic assembles or composites such as one-dimensional (1D) graphene aerogel fibers [12], two-dimensional (2D) graphene-based paper-like films [13-15], three-dimensional (3D) graphene-based polymer composites [16-23].

Because of the random stacking and aggregating characteristics of graphene sheets caused by their high aspect ratio and large specific surface area, dispersing graphene sheets uniformly into polymer matrices by mechanical stirring remains challenging, and percolation pathway among those isolated

graphene sheets also need to be established for efficient electron transport. Consequently, inferior electrical conductivities (1×10^{-7} to 1×10^{-1} S/cm) have been reported in previous work for graphene-based composites [12, 20-27]. Furthermore, poor dispersion of graphene sheets in matrices may cause fractures and weak interfaces within the composites that compromise the mechanical and thermal properties [28-34].

In order to resolve the issue associated with the poor graphene dispersion in polymer matrices, 3D monolithic graphene frameworks can be prepared before the incorporation of matrices. Several 3D macroscopic structures of graphene sheets have been developed such as hydrogels, sponges, foams and aerogels recently [12, 24, 30-31, 35-46], and related functional composites were prepared by direct infiltration of matrix into these monolithic structures. The overall properties of the composites have been improved (e.g., bulk electrical conductivity from 1×10^{-3} to 2.48×10^{-1} S/cm, thermal conductivity from 0.12 to 0.36 W/(m•K), and compressive strain reaching up to 60% [35-44]). Although 3D graphene monoliths and their composites show promising potential for practical applications [37, 40, 47-52], scanning electron microscope (SEM) images of their structures still indicate inefficient utilization of a substantial part of graphene sheets to form effective pathways for transport and disordered cross-linking of graphene sheets, resulting in properties (e.g., stiffness, strength, Young's Modulus, thermal and electrical conductivity) far below those of the individual graphene sheets as expected [45]. Moreover, the related graphene sheets used for fabrication of those 3D graphene structures exhibit small areas (smaller than a hundred square microns), which would lead to high inter-sheet contact resistance due to a high density of junctions. Therefore, further efforts are needed to fabricate graphene-based 3D structures with larger-scale features and more controllable processing. Significant opportunities remain to improve the utilization efficiency of monolithic graphene-based structures and their resultant properties.

The present work demonstrates the fabrication, characterization, and multifunctional performances of 3D GA-based polymer composites. Utilizing LGO synthesized by a modified Hummer's method as precursors, GA is prepared by a hydrothermal reduction and freeze-drying process, followed by thermal reduction [53]. The as-formed 3D highly porous GA frameworks present well-aligned interconnections among graphene sheets, high porosity, ultralight density, excellent electrical conductivity and ultralarge compressibility. By the direct infiltration process under ice-bath and vacuum assistances, PDMS is incorporated into GA to prepare 3D GAPC. The resulting highly multifunctional GAPC exhibits high electrical and thermal conductivity, ultralarge deformability, stable piezo-resistance effect, superior electric Joule heating performance, and good hydrophobicity.

2 MATERIAL FABRICATION

Graphite flakes (50 mesh) were purchased from Nanjing Xianfeng Nanomaterials Tech. Co., LTD (China), and PDMS (Sylgard 184) was supplied by Dow Corning Co., LTD (China). Using LGO sheets synthesized by a modified Hummer's method as precursors, GA was fabricated by a modified conventional hydrothermal approach, followed by freeze-drying and thermal reduction [53-54].

As illustrated in Fig. 1, PDMS matrix solution was self-infiltrated into as-prepared GA frameworks to fabricate 3D GAPC. To facilitate the infiltration process, PDMS solution was first prepared by mixing PDMS base agent, curing agent and n-hexane in the ratio of 10:1:1 by weight, followed by magnetic stirring for 30 min. Because PDMS maintains good fluidity at low temperatures, GA was immersed into the solution under vacuum and ice-bath conditions for 6 h to facilitate PDMS penetration into aerogel pores and to eliminate trapped bubbles. Subsequently, the wetted GAPC cylinder was taken out of solution and kept in a vacuum oven at 55 ^{o}C for 5h to solidify and remove the n-hexane. The resulting GAPC maintained the original physical structure without visible changes to the GA frameworks (e.g., shrinkage) as shown in Fig. 1.

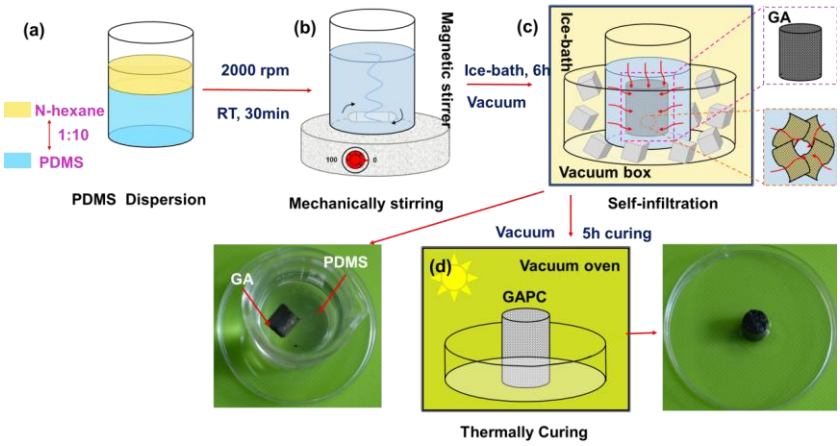

Figure 1 Fabrication process of GAPC. (a) Initial PDMS solution with curing agent and n-hexane in the ratio of 10:1:1 by weight; (b) mechanically stirring the PDMS solution; (c) self-infiltrating PDMS into GA porous frameworks under assistance of ice-bath and vacuum conditions; (d) thermally curing PDMS at 55℃ in vacuum.

3. RESULTS AND DISCUSSION

3.1 Characterization of materials

TEM images of isolated LOG sheets display typical wrinkled, few-layer structures with clear hexagonal patterns in selected-area electron diffraction (SAED) (see Fig. 2a and b), indicating the graphitic nature of the material. The AFM image in Fig. 2c shows an individual LGO sheet with a thickness of 0.8 nm, and optical image in Fig. S1e reveals average lateral length of several tens of micrometers to be 45±5 μm, leading to an ultralarge aspect ratio (≥50,000). This is beneficial to the self-assembly process of LGO sheets to form 3D GA frameworks. Fig. 2d displays an optical image of a GA sample with a cylindrical shape, and Fig. 2e shows well-aligned honeycomb-like 3D GA frameworks with pore sizes of tens of micrometers. From the cross-sectional images of GA frameworks, as depicted in Fig. 2f-g, graphene sheets first stack in a facial-linking pattern by strong π-π interactions with interfacial area of ~ 400 μm^2 (interfacial stacking length ~ 20±2 μm) during the freeze-drying process, and subsequently form a hierarchical porous structure.

The conjugated domains of LGO structures are gradually reduced by EDA during the hydrothermal process. The resulting hydrophobicity and Brownian movement force individual sheets to approach mutually, and then the strong π-π interactions among them facilitates self-assembly of LGO to form effective local cross-links first (X cross-link) and finally the rhombus framework (See Fig. 2 f and g) [38]. During the hydrothermal and in situ chemical reduction, those small-scale cross-links evolve into stacking over a larger extent strengthened by π-π interactions. As a result, totally self-supported and well-aligned 3D honeycomb graphene frameworks are formed, as shown in Fig. 2e.

To fabricate GAPC, a cylindrical GA sample is directly immersed into PDMS solution for the matrix self-infiltrating process, and the composite is finally obtained after thermal curring (see Fig. 2i and Fig. 1). SEM images of GAPC in Fig. 2j-k show that the cellular graphene walls in the GA framework and PDMS are interlaced together seamlessly by strong bonding, which is beneficial to the overall performance of GA-based composites (e.g., mechanical, electrical and thermal properties). As shown in the inset of Fig. 2j, GAPC exhibts better hydrophobicity with a water contact angle over 135o at RT which is larger than that of GA, implying that the GA-based composites are potential candidates for anti-ice or de-icing applications. They can also be reshaped as membrane-like materials coated on airfoils, wind turbines, or power grid transmission lines. Fig. 2l and m show the typical surface morphology of the wrinkling graphene sheets and well-cured PDMS matrix, respectivley.

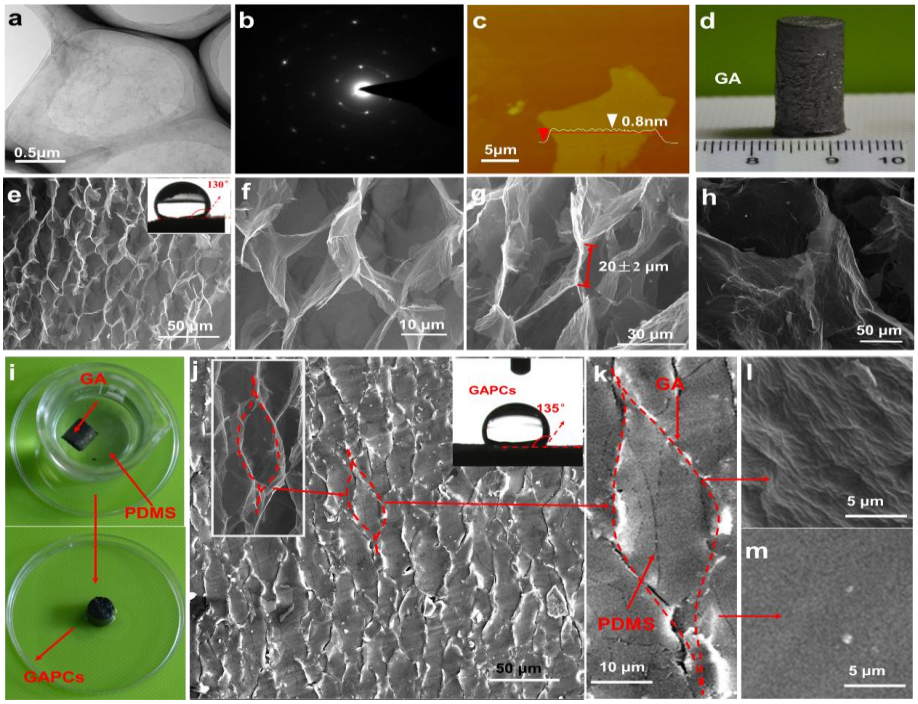

Figure 2 (a) TEM image of isolated LGO sheets; (b) SAED pattern of LGO; (c) AFM image of individual LGO sheet; (d) optical image of an as-formed GA; (e) SEM images of GA frameworks (10 mg/cm^3), the inset shows contact angle; (f) rhombus frameworks of graphene sheets in GA; (g) X joint feature of few-layer graphene sheets; (h) typical morphology of LGO sheets; (i) direct infiltration of PDMS into the porous GA frameworks; (j) SEM morphology of GAPC, the left inset shows the unit framework and the right presents contact angle; (k) a close-up of the boundary between the framework (GA) and matrix (PDMS); (l) typical morphology of graphene sheets in GAPC, (m) SEM image of PDMS in GAPC.

3.2 Electromechanical properties

The GA also exhibits an excellent electrical conductivity of 1.148 S/cm at an ultralow density (10 mg/cm^3), indicating promising potential as a framework for electrically conductive composites. As shown in Fig. 3a, the electrical conductivity of GAPC depends on the GA loading fraction and at 1 wt% (0.44 vol%) loading is 1 S/cm, which is 2 to 7 times higher than that of conventional graphene-based composites [17, 24-29,31,36, 38, 43]. The high electrical conductivity of GAPC is attributed to the well-interconnected GA frameworks.

GAPC exhibits excellent mechanical deformation and synchronous response of electric performance, making them suitable as stretchable conductors or sensitive strain gauges. As shown in Fig. 4a, a GAPC sample is pasted with silver conductive paint to minimize contact resistance, and sine-wave (0.1Hz) cyclic excitations are loaded using a MTS test machine under compressive strains of 20, 50 and 80%. Interestingly, Fig. 6c demonstrates that the resistivity of GAPC (GA=1 wt%) changes from 0 to +20% in response to compressive strains from 0 to 20%, which is opposite to that of GA (a decreasing resistivity within the range of 0 to -30%). This phenomenon can be explained as follows. The stacking area of interconnected graphene sheets in GA increases during the compressive process, resulting in more pathways for electron transport (see Fig. 4b). However, vertical compression (0 to 80% strain) generates radial expansion of the encapsulated PDMS (0 to 32% strain). As a result, the adjacent connected graphene sheets at the cellular corners of GA in GAPC are propped open partly by PDMS, which reduces electron transport channels in the composite during the compressive process (see Fig. 4c). The electro-mechanical properties of GAPC are studied under sine-wave (0.1 Hz) dynamic cyclic compression (see Fig. 3d), and the resistivity change ($|\Delta R/R|$)-compressive strain curves show typical non-linear behavior and completely recoverable resistivity response. The $|\Delta R/R|$ values of GAPC stabilize at 20, 53 and 90% after the 3rd, 4th and 8th cycle at compressive strains of 20, 50 and 80%, respectively.

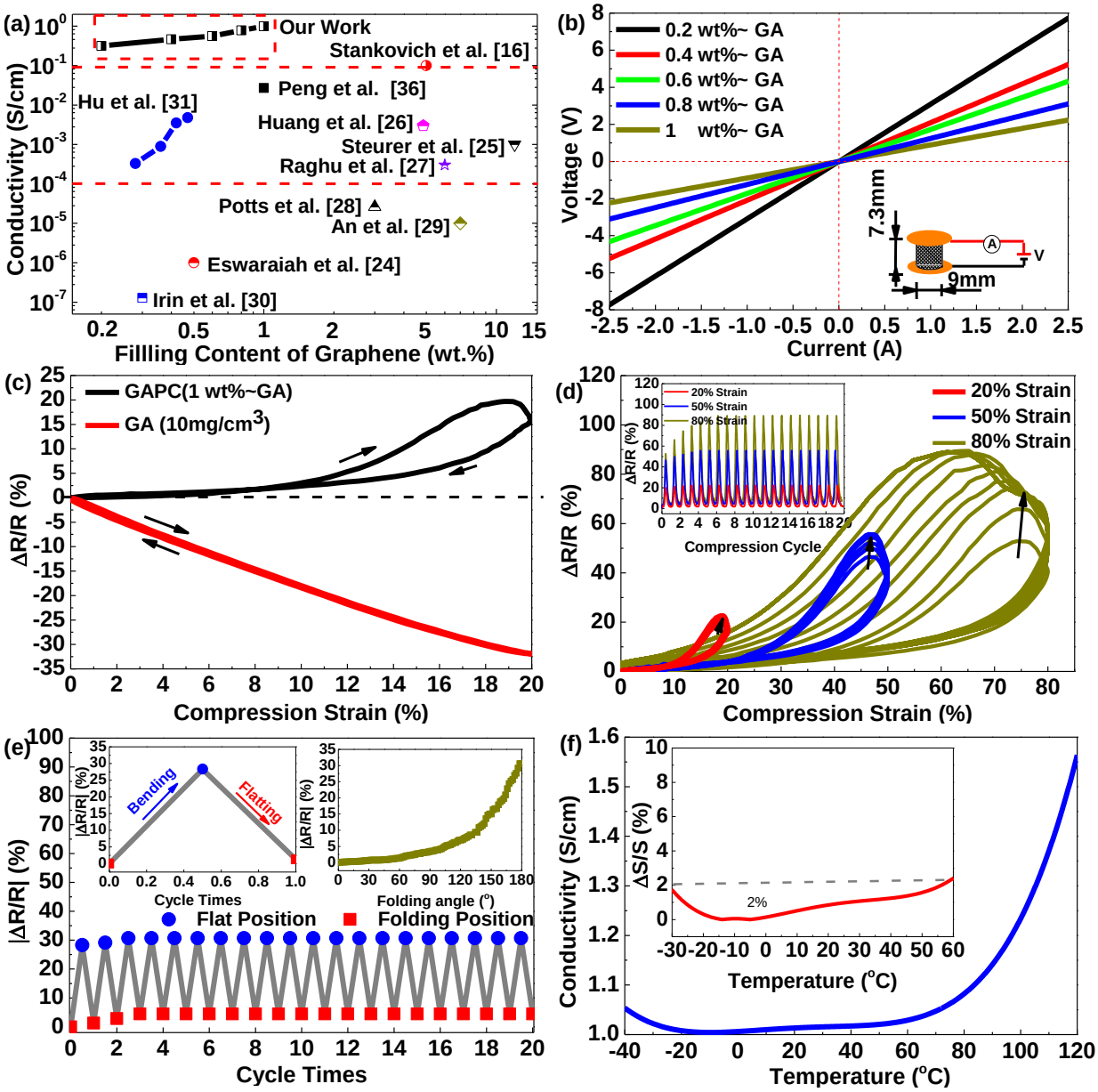

Figure 3 (a) Electrical conductivity of GAPC (GA content≤1 wt%) compared with other graphene-based composites; (b) I-V curves of GAPC; (c) piezoresistivity effect of GA and GAPC at a strain of 20%; (d) resistivity change and electro-mechanical stability of GAPC under cyclic compressive strains of 20, 50 and 80% respectively. The inset shows the resistance change of GAPC under 20 cycles of compression; (e) electro-mechanical properties of GAPC under a bending angle of 180° and 20 bending-flatting cycles. The left inset shows the resistance change under a bending-flatting cycle, while the right inset illuminates the resistance change when the bending angle changes from 0 to 180°; (f) temperature-dependent conductivity of GAPC with temperatures from -40 to 120 °C. The inset shows the conductivity change when the temperature increases from -30 to 60 °C.

To further understand the electro-mechanical properties of GAPC, the samples (GA=1 wt%) were bent 180° around a cylinder (diameter = 2.5 mm) to investigate the corresponding influence on resistivity. As shown in the right inset of Fig. 3e, |ΔR/R| first rises to 28% with a bending angle reaching up to 180° and then stabilizes at 30% at the 4th cycle. Through 20 folding-unfolding cycles, |ΔR/R| increases during the first four cycles and then almost stabilizes until the 20th cycle with a variation of ±5%, which is possibly due to the absence of significant structural damage (e.g., cracks on graphene sheets) of the GA frameworks (see Fig. 3e). Overall, GAPC shows better

electro-mechanical stability and electrical sensitivity than other reported graphene-based composites under external deformation conditions [13, 16, 24-31].

To thoroughly understand the electron transport mechanisms in GAPC, the impact of temperature fluctuations on electrical conductivity is studied (see Fig. 3f). A typical GAPC sample (GA=1 wt%) is heated controllably from -40 to 120 ^{o}C at a heating rate of 0.5 ^{o}C/min in a furnace. The conductivity shows good stability from -40 to 60 ℃ with a slight variation of 2%, and increases from 1.02 S/cm at -40 ^{o}C to 1.55 S/cm at 120 ^{o}C. This negative temperature coefficient of expansion (NTCE) effect indicates typical semiconductor behavior with temperature dependence of resistivity and conductivity, which is due to the existence of potential barriers between highly conductive conjugation domains on reduced graphene sheets.

The transport mechanism of thermally activated electrons in GA is believed to be governed by a dual 2D/3D hopping conduction mechanism (2D in basal plane of graphene sheets: $\ln\rho \propto T^{-[1/(2+1)]}$, 3D in stacked interfaces among graphene sheets: $\ln\rho \propto T^{-[1/(3+1)]}$, where ρ is the resistivity and T is temperature), similar to that of other nanostructures (e.g., carbon Nanotubes and GA fibers) [12, 54]. However, the electrical conductivity of GAPC shows weaker temperature dependence and better stability than that of GA, and this behavior is beneficial to their application at low temperatures (<0 ^{o}C). Consequently, the excellent electro-mechanical properties and temperature-resistivity effects of GAPC show potential for applications in high-performance stretchable conductors with high sensitivity and long-term stability.

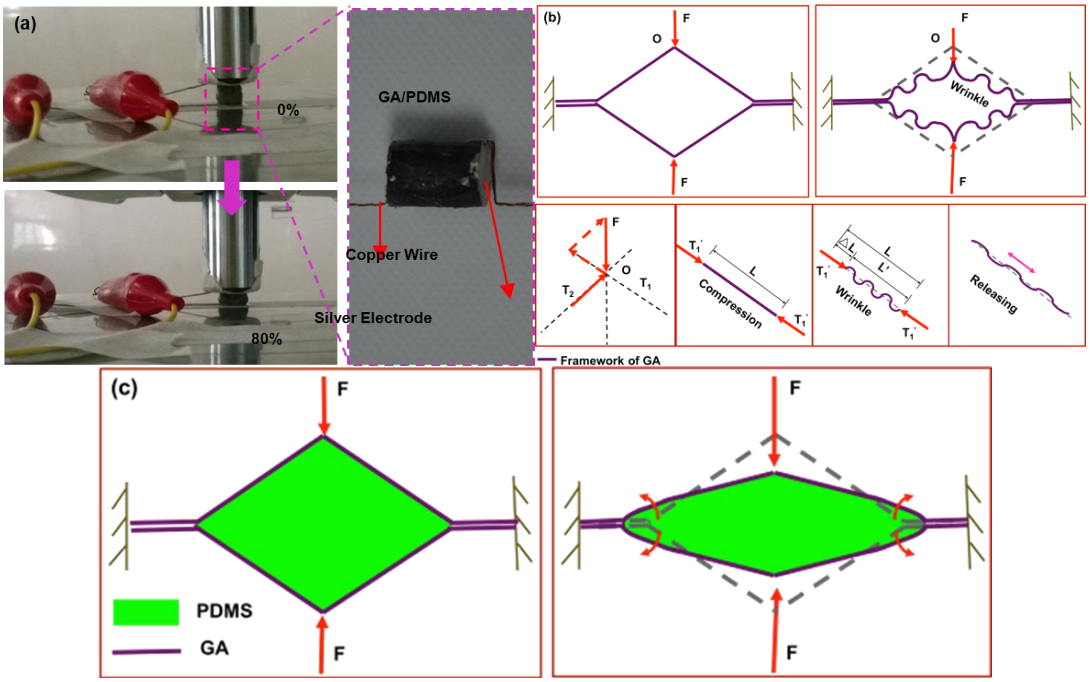

Figure 4 (a) Snapshots of GAPC for piezoresistivity tests; (b)-(c) conceptual illustrations of negative piezoresistivity effect for GA and positive piezoresistivity effect for GAPC.

4. Conclusions

In this work, GA-based multifunctional polymer composites with excellent electro-mechanical properties were fabricated and characterized. The 3D GA frameworks were prepared by a hydrothermal reduction of large-scale graphene oxide (LGO) sheets, followed by freeze-drying and thermal reduction. These GA frameworks exhibit ultralight density, ultra-high compressibility, stable electro-mechanical properties and excellent electrical conductivity. By a direct infiltration process, GA was combined with PDMS matrix to fabricate the polymer composites with multifunctional properties. The as-prepared GAPC shows high electrical conductivity, outstanding electro-mechanical and stable piezo-resistance effec, which makes them promising in practical

applications such as stretchable electronic devices, ultralarge strain sensors.

References

[1] Novoselov, K. S., Geim, A. K., Morozov, S. V., Jiang, D., Zhang, Y., Dubonos, S. V., Firsov, A. A. (2004). Electric field effect in atomically thin carbon films. Science. **306:5696**, 666-669.

[2] Geim, A. K., Novoselov, K. S. (2007). The rise of graphene. Nature Mater. **6:3**, 183-191.

[3] Geim, A. K. (2009). Graphene: Status and Prospects. Science. **324:5934**, 1530-1534.

[4] Balandin, A. A., Ghosh, S., Bao, W., Calizo, I., Teweldebrhan, D., Miao, F., et al. (2008). Superior thermal conductivity of single-layer graphene. Nano Letters. **8:3**, 902-907.

[5] Bolotin, K. I., Sikes, K. J., Jiang, Z., Klima, M., Fudenberg, G., Hone, J., et al. (2008). Ultrahigh electron mobility in suspended graphene. Solid State Communications. **146:9**, 351-355.

[6] Stoller, M. D., Park, S., Zhu, Y., An, J., Ruoff, R. S. (2008). Graphene-based ultracapacitors. Nano letters. **8: 10**, 3498-3502.

[7] Nair, R. R., Blake, P., Grigorenko, A. N., Novoselov, K. S., Booth, T. J., Stauber, T., et al. (2008). Fine structure constant defines visual transparency of graphene. Science. **320:5881**, 1308-1308.

[8] Lee, C., Wei, X., Kysar, J. W., Hone, J. (2008). Measurement of the elastic properties and intrinsic strength of monolayer graphene. Science. **321:5887**, 385-388.

[9] Park, S., Ruoff, R. S. (2009). Chemical Methods for the Production of Graphenes. Nature Nanotechnology. **4:4**, 217-224.

[10] Dreyer, D. R., Park, S., Bielawski, C. W., Ruoff, R. S. (2010). The Chemistry of Graphene Oxide. Chemical Society Reviews. **39:1**, 228-240.

[11] Xiong, G., Hembram, K. P. S. S., Zakharov, D. N., Reifenberger, R. G., Fisher, T. S. (2012). Controlled thin graphitic petal growth on oxidized silicon. Diamond and Related Materials. **27:28**, 1-9.

[12] Xu, Z., Zhang, Y., Li, P., Gao, C. (2012). Strong, conductive, lightweight, neat graphene aerogel fibers with aligned pores. ACS Nano. **6:8**, 7103-7113.

[13] Xu, Y., Hong, W., Bai, H., Li, C., Shi, G. (2009). Strong and ductile poly (vinyl alcohol)/graphene oxide composite films with a layered structure. Carbon. **47:15**, 3538-3543.

[14] Dikin, D. A., Stankovich, S., Zimney, E. J., Piner, R. D., Dommett, G. H., Evmenenko, G., et al. (2007). Preparation and characterization of graphene oxide paper. Nature. **448:7152**, 457-460.

[15] Xiong, G., Meng, C., Reifenberger, R. G., Irazoqui, P. P., Fisher, T. S. (2014). A Review of Graphene-Based Electrochemical Microsupercapacitors. Electroanalysis. **26**, 30-51.

[16] Stankovich, S., Dikin, D. A., Dommett, G. H., Kohlhaas, K. M., Zimney, E. J., Stach, E. A., et al. (2006). Graphene-based composite materials. Nature. **442:7100**, 282-286.

[17] Ramanathan, T., Abdala, A. A., Stankovich, S., Dikin, D. A., Herrera-Alonso, M., Piner, R. D., et al. (2008). Functionalized graphene sheets for polymer nanocomposites. Nature Nanotechnology. **3:6**, 327-331.

[18] Compton, O. C., Nguyen, S. T. (2010). Graphene Oxide, Highly Reduced Graphene Oxide, and Graphene: Versatile Building Blocks for Carbon-Based Materials. Small. **6:6**, 711-723.

[19] Bai, H., Li, C., Shi, G. (2011). Functional composite materials based on chemically converted graphene. Advanced Materials. **23:9**, 1089-1115.

[20] Zhu, Y., Murali, S., Cai, W., Li, X., Suk, J. W., Potts, J. R., et al. (2010). Graphene and graphene oxide: synthesis, properties, and applications. Advanced Materials. **22:35**, 3906-3924.

[21] Huang, X., Qi, X., Boey, F., Zhang, H. (2012). Graphene-based composites. Chemical Society Reviews. **41:2**, 666-686.

[22] Li, X., Cai, W., An, J., Kim, S., Nah, J., Yang, D., et al. (2009). Large-area synthesis of high-quality and uniform graphene films on copper foils. Science. **324:5932**, 1312-1314.

[23] Park, S., Ruoff, R. S. (2009). Chemical methods for the production of graphenes. Nature Nanotechnology. **4:4**, 217-224.

[24] Eswaraiah, V., Sankaranarayanan, V., Ramaprabhu, S. (2011). Functionalized graphene–PVDF foam composites for EMI shielding. Macromolecular Materials and Engineering. **296:10**, 894-898.

[25] Steurer, P., Wissert, R., Thomann, R., et al. (2009). Functionalized graphenes and thermoplastic nanocomposites based upon expanded graphite oxide. Macromolecular Rapid Communications. **30:4-5**, 316-327.

[26] Huang, Y., Qin, Y., Zhou, Y. (2010). Polypropylene/graphene oxide nanocomposites prepared by in situ Ziegler− Natta polymerization. Chemistry of Materials. **22:13**, 4096-4102.

[27] Raghu, A. V., Lee, Y. R., Jeong, H. M., Shin, C. M. (2008). Preparation and physical properties of waterborne polyurethane/functionalized graphene sheet nanocomposites. Macromolecular Chemistry and Physics. **209:24**, 2487-2493.

[28] Potts, J. R., Murali, S., Zhu, Y., Zhao, X., Ruoff, R. S. (2011). Microwave-exfoliated graphite

oxide/polycarbonate composites. Macromolecules. **44:16**, 6488-6495.
[29] An, J. E., Jeong, Y. G. (2013). Structure and electric heating performance of graphene/epoxy composite films. European Polymer Journal. **49:6**, 1322-1330.
[30] Irin, F., Das, S., Atore, F. O., Green, M. J. (2013). Ultralow percolation threshold in aerogel and cryogel templated composites. Langmuir. **29:36**, 11449-11456.
[31] Hu, H., Zhao, Z., Zhang, R., Bin, Y., Qiu, J. (2014). Polymer casting of ultralight graphene aerogels for the production of conductive nanocomposites with low filling content. Journal of Materials Chemistry A. **2:11**, 3756-3760.
[32] Veca, L. M., Meziani, M. J., Wang, W., Lu, F., Zhang, P., et al. (2009). Carbon nanosheets for polymeric nanocomposites with high thermal conductivity. Advanced Materials. **21:20**, 2088-2092.
[33] Yu, A., Ramesh, P., Sun, X., Bekyarova, E., Itkis, M. E., Haddon, R. C. (2008). Enhanced thermal conductivity in a hybrid graphite nanoplatelet–carbon nanotube filler for epoxy composites. Advanced Materials. **20:24**, 4740-4744.
[34] Ganguli, S., Roy, A. K., Anderson, D. P. (2008). Improved thermal conductivity for chemically functionalized exfoliated graphite/epoxy composites. Carbon. **46:5**, 806-817.
[35] Xu, Y., Sheng, K., Li, C., Shi, G. (2010). Self-assembled graphene hydrogel via a one-step hydrothermal process. ACS Nano. **4:7**, 4324-4330.
[36] Peng, Q., Li, Y., He, X., Gui, X., Shang, Y., Wang, C., et al. (2014). Graphene Nanoribbon Aerogels Unzipped from Carbon Nanotube Sponges. Advanced Materials. **26:20**, 3241-3247.
[37] Zhang, X., Sui, Z., Xu, B., Yue, S., Luo, Y., Zhan, W., Liu, B. (2011). Mechanically strong and highly conductive graphene aerogel and its use as electrodes for electrochemical power sources. Journal of Materials Chemistry. **21:18**, 6494-6497.
[38] Zhang, L., Chen, G., Hedhili, M. N., Zhang, H., Wang, P. (2012). Three-dimensional assemblies of graphene prepared by a novel chemical reduction-induced self-assembly method. Nanoscale. 4:22, 7038-7045.
[39] Huang, H., Chen, P., Zhang, X., Lu, Y., Zhan, W. (2013). Edge-to-Edge Assembled Graphene Oxide Aerogels with Outstanding Mechanical Performance and Superhigh Chemical Activity. Small. **9:8**, 1397-1404.
[40] Hu, H., Zhao, Z., Wan, W., Gogotsi, Y., Qiu, J. (2014). Polymer/Graphene Hybrid Aerogel with High Compressibility, Conductivity, and "Sticky" Superhydrophobicity. ACS Applied Materials & Interfaces. **6:5**, 3242-3249.
[41] Ahn, H. S., Jang, J. W., Seol, M., Kim, J. M., Yun, D. J., Park, C., et al. (2013). Self-assembled foam-like graphene networks formed through nucleate boiling. Scientific Reports 2013; **3**.
[42] Sun, H., Xu, Z., Gao, C. (2013). Multifunctional, Ultra - Flyweight, Synergistically Assembled Carbon Aerogels. Advanced Materials. 25:18, 2554-2560.
[43] Tang, G., Jiang, Z. G., Li, X., et al. (2014). Three dimensional graphene aerogels and their electrically conductive composites. Carbon. **77**, 592–599.
[44] Fan, Z., Marconnet, A., Nguyen, S. T., Lim, C. Y., Duong, H. M. (2014). Effects of heat treatment on the thermal properties of highly nanoporous graphene aerogels using the infrared microscopy technique. International Journal of Heat and Mass Transfer. **76**: 122-127.
[45] Wu, Z., Ren, W., Gao, L., Zhao, J., Chen, Z., Liu, B., et al. (2009). Synthesis of graphene sheets with high electrical conductivity and good thermal stability by hydrogen arc discharge exfoliation. ACS Nano. **3:2**, 411-417.
[46] Lu, A. H., Hao, G. P., Sun, Q. (2013). Design of Three-Dimensional Porous Carbon Materials: From Static to Dynamic Skeletons. Angewandte Chemie International Edition. **52:31**, 7930-7932.
[47] Chen, J., Sheng, K. X., Luo, P. H., Li, C., Shi, G. Q. (2012). Graphene hydrogels deposited in nickel foams for high-rate electrochemical capacitors. Advanced Materials. **24**, 4569–4573
[48] Zhu, Z., Garcia-Gancedo, L., Flewitt, A. J., Xie, H., Moussy, F., Milne, W. I. (2013). A critical review of glucose biosensors based on carbon nanomaterials: Carbon nanotubes and graphene. Sensors. **12:5**, 5996-6022.
[49] Singh, G., Choudhary, A., Haranath, D., Joshi, A. G., Singh, N., Singh, S., Pasricha, R. (2012). ZnO decorated luminescent graphene as a potential gas sensor at room temperature. Carbon. **50:2**, 385-394.
[50] Huang, X., Yin, Z., Wu, S., Qi, X., He, Q., Zhang, Q., et al. (2011). Graphene-Based Materials: Synthesis, Characterization, Properties, and Applications. Small. **7:1**4, 1876-1902.
[51] Zhao, J., Ren, W., Cheng, H. M. (2012). Graphene sponge for efficient and repeatable adsorption and desorption of water contaminations. Journal of Materials Chemistry. **22:38**, 20197-20202.
[52] Bi, H., Xie, X., Yin, K., Zhou, Y., Wan, S., He, L., et al. (2012). Spongy graphene as a highly efficient and recyclable sorbent for oils and organic solvents. Advanced Functional Materials. **22:21**, 4421-4425.
[53] Xu, X., Li, H., Zhang, Q., Hu, H., Zhao, Z., Li, J. et al. (2015). Self-Sensing, Ultralight and Conductive 3D Graphene/Iron Oxide Aerogel Elastomer Deformable in Magnetic Field. ACS nano. **9:4**, 3969–3977
[54] Zhang, Q., Xu, X., Li, H., Xiong, G., Hu, H., Fisher, T. S. (2015). Mechanical robustness graphene aerogel multifunctional polymer composites. Carbon. **93:c**, 659-670.